Parkin is a lipid-responsive regulator of fat uptake in mice and mutant human cells

Kye-Young Kim,[1] Mark V. Stevens,[1] M. Hasina Akter,[1] Sarah E. Rusk,[1] Robert J. Huang,[1] Alexandra Cohen,[1] Audrey Noguchi,[2] Danielle Springer,[2] Alexander V. Bocharov,[3] Tomas L. Eggerman,[3] Der-Fen Suen,[4] Richard J. Youle,[4] Marcelo Amar,[5] Alan T. Remaley,[5] and Michael N. Sack[1]

[1]Center for Molecular Medicine, National Heart, Lung, and Blood Institute (NHLBI), [2]Mouse Phenotyping Core, NHLBI, [3]NIH Clinical Center, [4]Biochemistry Section, Surgical Neurology Branch, National Institute of Neurological Disorders and Stroke (NINDS), and [5]Cardio-Pulmonary Medicine Branch, NHLBI, Bethesda, Maryland, USA.

It has long been hypothesized that abnormalities in lipid biology contribute to degenerative brain diseases. Consistent with this, emerging epidemiologic evidence links lipid alterations with Parkinson disease (PD), and disruption of lipid metabolism has been found to predispose to α-synuclein toxicity. We therefore investigated whether Parkin, an E3 ubiquitin ligase found to be defective in patients with early onset PD, regulates systemic lipid metabolism. We perturbed lipid levels by exposing *Parkin*$^{+/+}$ and *Parkin*$^{-/-}$ mice to a high-fat and -cholesterol diet (HFD). *Parkin*$^{-/-}$ mice resisted weight gain, steatohepatitis, and insulin resistance. In wild-type mice, the HFD markedly increased hepatic Parkin levels in parallel with lipid transport proteins, including CD36, Sr-B1, and FABP. These lipid transport proteins were not induced in *Parkin*$^{-/-}$ mice. The role of Parkin in fat uptake was confirmed by increased oleate accumulation in hepatocytes overexpressing Parkin and decreased uptake in *Parkin*$^{-/-}$ mouse embryonic fibroblasts and patient cells harboring complex heterozygous mutations in the Parkin-encoding gene *PARK2*. Parkin conferred this effect, in part, via ubiquitin-mediated stabilization of the lipid transporter CD36. Reconstitution of Parkin restored hepatic fat uptake and CD36 levels in *Parkin*$^{-/-}$ mice, and Parkin augmented fat accumulation during adipocyte differentiation. These results demonstrate that Parkin is regulated in a lipid-dependent manner and modulates systemic fat uptake via ubiquitin ligase–dependent effects. Whether this metabolic regulation contributes to premature Parkinsonism warrants investigation.

Introduction

PARK2 mutations associate with an autosomal recessive juvenile form of Parkinson disease (PD) (1). However, the role of Parkin in the development of PD in mice is surprisingly modest, as the genetic deletion of Parkin (2, 3) and the combined KO of Parkin with additional "candidate Parkinson susceptibility genes" *PINK1* and *DJ-1* do not substantially replicate the human condition (4). These unexpected findings suggest that the biological function of Parkin may not primarily modulate neurodegeneration but rather that *PARK2* mutations increase biological susceptibility to stressors that manifest with substantia nigra neurodegeneration. Thus, the characterization of the functional actions of Parkin could be instrumental in delineating its role in the pathophysiology underpinning the development of PD.

Parkin encodes an E3 ubiquitin protein ligase and contains 465 amino acids with multiple distinct domains, including a ubiquitin-like domain, a unique Parkin-specific domain, 2 RING domains, and an in-between-RING domain (5). The structure of this protein with its multiple binding domains is most likely central to the myriad of functions prescribed to Parkin (6). Additionally, the subcellular location of Parkin appears to be dynamic, with a predominant cytosolic localization with redistribution to the nucleus (7) and to the outer mitochondrial membrane (8, 9). Parkin exhibits mono- and multiubiquitination functions (10), and studies show that classical as well as nonclassical ubiquitin linkages facilitate proteosome-dependent and independent Parkin effects (11–14).

An emerging body of evidence suggests that lower levels of cholesterol and fatty acids associate with an increased risk of PD (15–17). Furthermore, it has long been hypothesized that abnormalities in lipid biology contribute to degenerative brain diseases and that the substantia nigra region has distinct phospholipid metabolism compared with other brain regions (18). It is interesting to note that the mutation of yeast genes controlling lipid metabolism augments α-synuclein toxicity, a central component of inclusion bodies in PD (19). Given these associations, it is intriguing that Parkin deletion in mice results in blunting of age-associated weight gain prior to evidence of other abnormalities (20). The mechanism underlying this phenotype has yet to be elucidated. Therefore, we hypothesized that Parkin may function in the biologic control of fat and/or cholesterol metabolism. To explore the role of Parkin in lipid biology, we characterized the systemic metabolic responses of Parkin WT (*Parkin*$^{+/+}$) and KO (*Parkin*$^{-/-}$) mice following the introduction of an equicaloric high-fat and -cholesterol diet (HFD).

In this study, we show that the *Parkin*$^{-/-}$ mice are profoundly resistant to HFD-induced weight gain. This phenotype does not result from the futile catabolism of nutrients or increased energy requirements, but rather is due to alterations in lipid metabolism. Although the alterations in fat accumulation are systemic, our initial characterization of the role of Parkin in regulating lipid metabolism focused on the liver. In response to HFD feeding, the *Parkin*$^{+/+}$ mice showed robust increases in Parkin levels, in parallel with elevated lipid transport proteins, increased hepatosteatosis, hepatic insulin resistance, and steatohepatitis. However, the *Parkin*$^{-/-}$ mice resisted all of these dietary phenotypic responses. In addition, gain- and loss-of-function studies in cell culture show

Conflict of interest: The authors have declared that no conflict of interest exists.
Citation for this article: *J Clin Invest.* 2011;121(9):3701–3712. doi:10.1172/JCI44736.

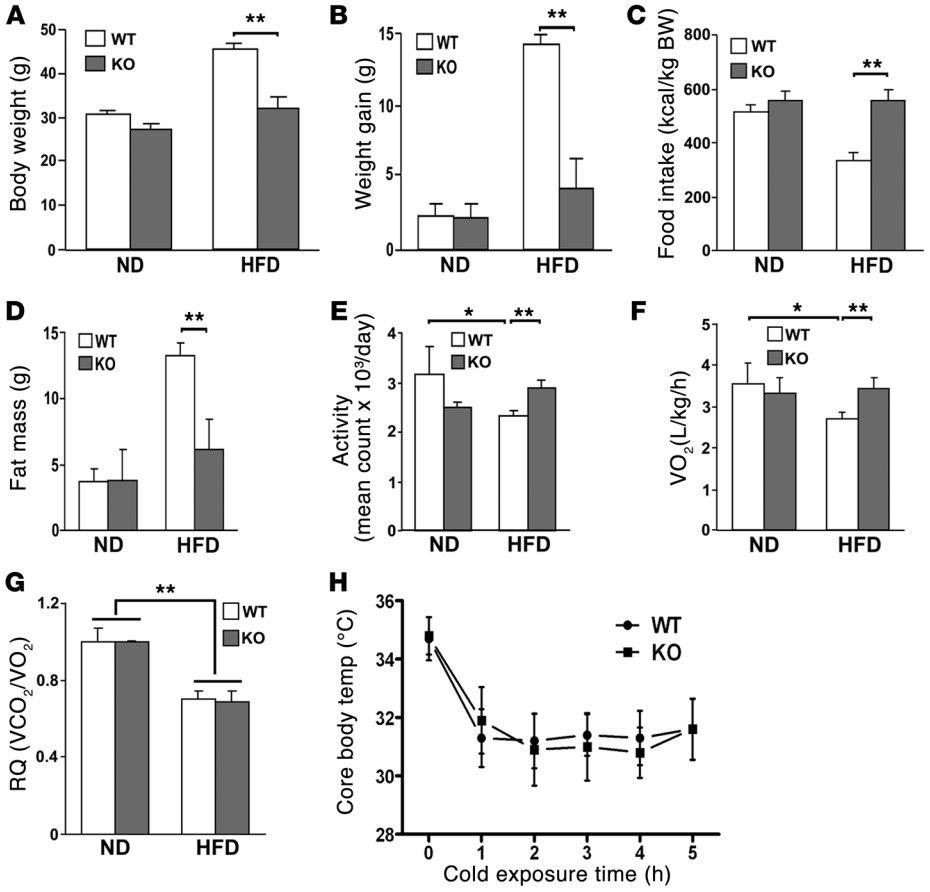

Figure 1

Parkin$^{-/-}$ mice (KO) are resistant to HFD-induced weight gain and have preserved activity and oxygen consumption. 12-week-old male mice were fed a ND or a HFD. BW (**A**) and weight gain (**B**) measured after 6.5 weeks of the ND compared with the HFD. (**C**) Daily food intake (kcal/kg BW) was measured for 3 days while mice were housed in a metabolic chamber. The mice were fed a ND or a HFD for 5 weeks prior to analysis. (**D**) Total body fat mass was analyzed by NMR spectroscopy. (**E**) Daily total movement counted by DSI telemetry system and averaged over 3 days. (**F**) Total metabolic rate (O_2 consumption) monitored by Oxymax system for 24 hours. VO_2, volume of O_2 consumed. (**G**) Respiratory quotient (RQ) measured for 24 hours. VCO_2, volume of CO_2 consumed. (**H**) Core body temperature response to a hypothermia challenge (4°C for 5 hours). Data are expressed as mean ± SD (n = 5–9 per group). $^*P < 0.05$; $^{**}P < 0.01$, compared with the corresponding controls.

that Parkin facilitated fat uptake with increased protein stability of the CD36 lipid transport protein. Interestingly, this reduction of fat uptake is mirrored in B cells derived from patients harboring complex heterozygous *PARK2* mutations who presented with premature Parkinsonism. The role of Parkin in modulating CD36 levels and lipid uptake was further evident by blunted upregulation of neuronal CD36 levels in response to the HFD in *Parkin*$^{-/-}$ mice and the reduction in lipid accumulation during adipocyte differentiation in *Parkin*$^{-/-}$ mouse embryonic fibroblasts (MEFs) and in Parkin-depleted 3T3-L1 cells. Furthermore, the reconstitution of CD36 in *Parkin*$^{-/-}$ mouse livers augmented hepatic fat uptake and the induction of Parkin-restored endogenous CD36 levels and lipid accumulation in *Parkin*$^{-/-}$ mice. Together these results provide extensive evidence showing that Parkin is a lipid-sensitive regulator of systemic fat metabolism and perturbations in this metabolism warrant exploration in the pathophysiology of *PARK2* mutation–mediated premature PD.

Results

Parkin$^{-/-}$ *mice resist nutrient-dependent weight gain without modulation in food intake or thermogenesis.* As *Parkin*$^{-/-}$ mice showed blunted weight gain with aging on a normal chow diet (ND) (20), we began by exploring whether this effect would be exacerbated on the HFD compared with matched WT control mice. At 12 weeks of age on the ND, Parkin WT and *Parkin*$^{-/-}$ mice showed no differences in weight or food intake (data not shown). Interestingly, these similarities were maintained at 18 weeks of age on the ND with similar increases in weight gain (Figure 1, A and B). In contrast, the introduction of the HFD resulted in robust weight gain and a concomitant reduction in food intake in the WT mice, whereas *Parkin*$^{-/-}$ mice were resistant to weight gain despite maintenance of food intake (Figure 1, A–C). The resistance to HFD-induced weight gain in *Parkin*$^{-/-}$ mice was supported by lower fat content as measured by NMR spectroscopy (Figure 1D). Interestingly, the WT mice became less active with diminished oxygen consumption, whereas *Parkin*$^{-/-}$ mice maintained their activity and oxygen consumption levels on the HFD (Figure 1, E and F). Due to their similar oxygen consumption rates on the ND, the differences in indirect calorimetry on the HFD probably reflect their differences in activity. In response to HFD, *Parkin*$^{+/+}$ and *Parkin*$^{-/-}$ mice showed a blunting of their respiratory quotient, a change compatible with increased fat metabolism (Figure 1G). The representative metabolic parameters from Parkin WT and *Parkin*$^{-/-}$ mice are shown in Supplemental Table 1 (supplemental material available online with this article; doi:10.1172/JCI44736DS1). Interestingly, resistance to weight gain was not due to futile thermogenesis, as the basal core body temperature and the reduction in core temperature in response to a hypothermic stress were the same in both genotypes (Figure 1H).

Parkin$^{-/-}$ *mice resilience to weight gain is paralleled by preserved insulin sensitivity and liver function.* The resistance to weight gain in *Parkin*$^{-/-}$ mice should manifest with resistance to HFD-induced metabolic dysfunction and to the development of insulin resistance. To investigate this, we measured parameters of glucose and insulin action. In parallel with the lack of difference in fat mass on the ND, fasting serum glucose levels were similar in both genotypes (Figure 2A). Interestingly, in parallel with the differential fat accumulation on

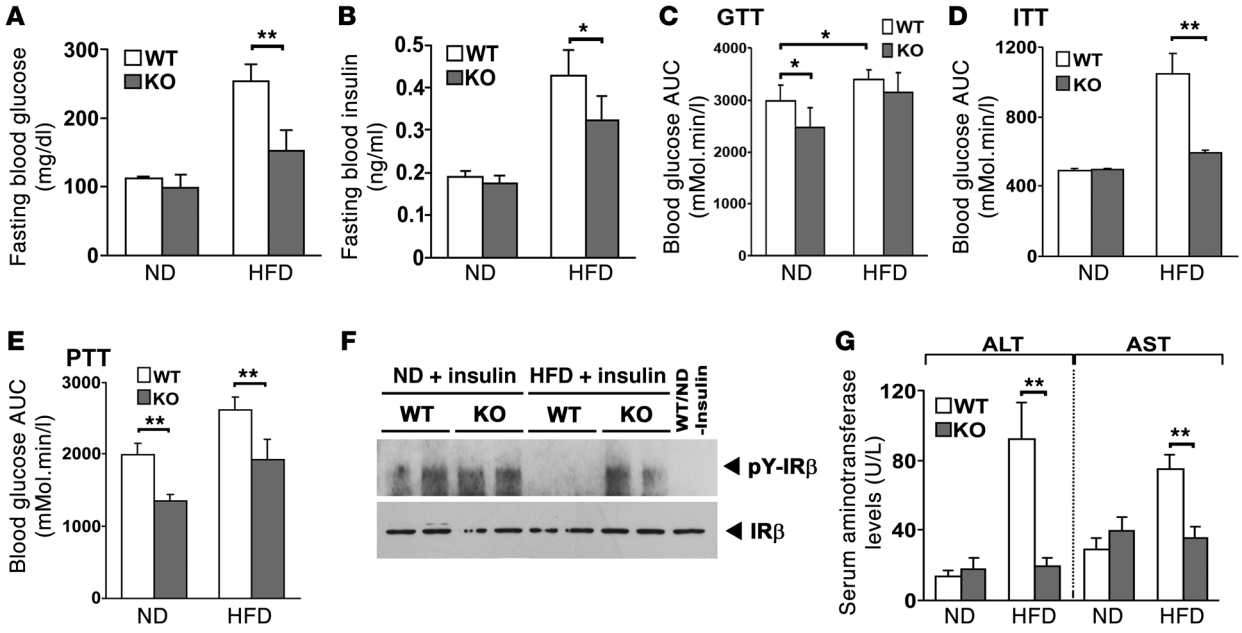

Figure 2

Parkin$^{-/-}$ mice are resistant to HFD-induced glucose intolerance and hepatic insulin resistance. (**A** and **B**) Fasting blood glucose and serum insulin levels in *Parkin*$^{+/+}$ and *Parkin*$^{-/-}$ mice. (**C**) GTT expressed as the AUC of blood glucose levels during the 2 hour study. (**D**) ITT expressed as AUC for blood glucose over 2 hours. (**E**) PTT expressed as AUC for blood glucose of 2 hours. (**F**) Assessment of phosphorylation of IRβ in liver following intraperitoneal insulin administration. Liver extracts were IP with IRβ antibody and the immunoblot performed with a phospho-tyrosine antibody. The far right lane shows protein expression in WT mice on the ND without insulin. (**G**) Serum aminotransferase levels. The mice were fed with ND or HFD for 6.5 weeks. Data are expressed as mean ± SD. *$P < 0.05$; **$P < 0.01$ versus controls (n = 4–6 per group).

the HFD, there was a significant induction of fasting serum glucose levels in the WT mice, with only a modest increase in the KO mice on the HFD (Figure 2A). The same pattern was evident when measuring fasting insulin levels, with a robust induction in the WT mice on the HFD and a more modest increase in the absence of Parkin (Figure 2B). Although there was no obvious phenotypic difference or genotype-specific increase in skeletal muscle fat accumulation (data not shown), the glucose tolerance test (GTT) showed impaired relative glucose tolerance in the WT mice on the ND and HFD (Figure 2C and Supplemental Figure 1A). In contrast, glucose dissipation in response to the insulin tolerance test (ITT) was similar in both genotypes on the ND and became impaired in the WT mice while remaining within the normal range in the KO mice in response to the HFD (Figure 2D and Supplemental Figure 1B). As fasting glucose levels reflect, in part, the control of hepatic gluconeogenesis, we assessed the rate of gluconeogenesis by the pyruvate tolerance test (PTT). Interestingly, *Parkin*$^{-/-}$ mice showed markedly diminished hepatic gluconeogenesis irrespective of the dietary composition (Figure 2E). To confirm that these serological findings were correlated with improved insulin signaling, hepatic insulin-responsive phosphorylation of the insulin receptor β (IRβ) was assayed in vivo. Phosphorylation of IRβ in *Parkin*$^{+/+}$ mice was significantly impaired on the HFD. while insulin signaling was sustained in the *Parkin*$^{-/-}$ mice on the ND and HFD (Figure 2F). Improved hepatic insulin sensitivity would also be expected to associate with a less HFD-induced hepatic steatohepatitis. We showed that serological markers reflecting steatohepatitis, i.e., alanine aminotransferase (ALT) and aspartate aminotransferase (AST), were elevated in *Parkin*$^{+/+}$ mice but not in *Parkin*$^{-/-}$ mice on the HFD (Figure 2G).

Parkin deficiency attenuates HFD-mediated adipose accumulation. To interrogate the mechanism underlying resistance to weight gain and insulin resistance in *Parkin*$^{-/-}$ mice, we evaluated whether attenuation in adipose accumulation was systemic or tissue specific. Adipose stores were uniformly lower in epididymal white adipose tissue, in interscapular brown fat deposits, and in subcutaneous tissue in KO mice compared with WT controls on the HFD (Figure 3, A–C). As the liver is highly susceptible to ectopic lipid accumulation, we investigated fat and cholesterol stores in the liver. On the ND, there is minimal fat storage in the liver as assessed by Oil Red O staining (Supplemental Figure 2A). Fat and cholesterol accumulation were markedly increased in the WT mice in response to HFD feeding and substantially less pronounced in *Parkin*$^{-/-}$ mice (Figure 3D). These histological findings were mirrored by the direct measurement of hepatocyte triglyceride (TG) and cholesterol content (Figure 3E and Supplemental Figure 2B). The levels of fasting serum-free fatty acids were significantly albeit modestly lower in *Parkin*$^{-/-}$ mice on the HFD (Figure 3F). In parallel, the *Parkin*$^{-/-}$ mice showed a markedly greater increase in TG content in feces samples collected over 72 hours compared with *Parkin*$^{+/+}$ mice on the HFD (Figure 3G). A similar pattern was evident by measuring cholesterol levels with diminished fasting serum levels in *Parkin*$^{-/-}$ mice on the HFD (Supplemental Figure 2C) in parallel with markedly increased fecal cholesterol content in the KO mice on the HFD (Supplemental Figure 2D).

Parkin modulates cellular fat uptake in response to oleate administration. The combination of diminished systemic adipose fat content, decreased serum-free fatty acid levels, and increased fecal TG levels in *Parkin*$^{-/-}$ mice on the HFD would support a role for Parkin in modulating cellular fat uptake. To investigate mechanisms underpin-

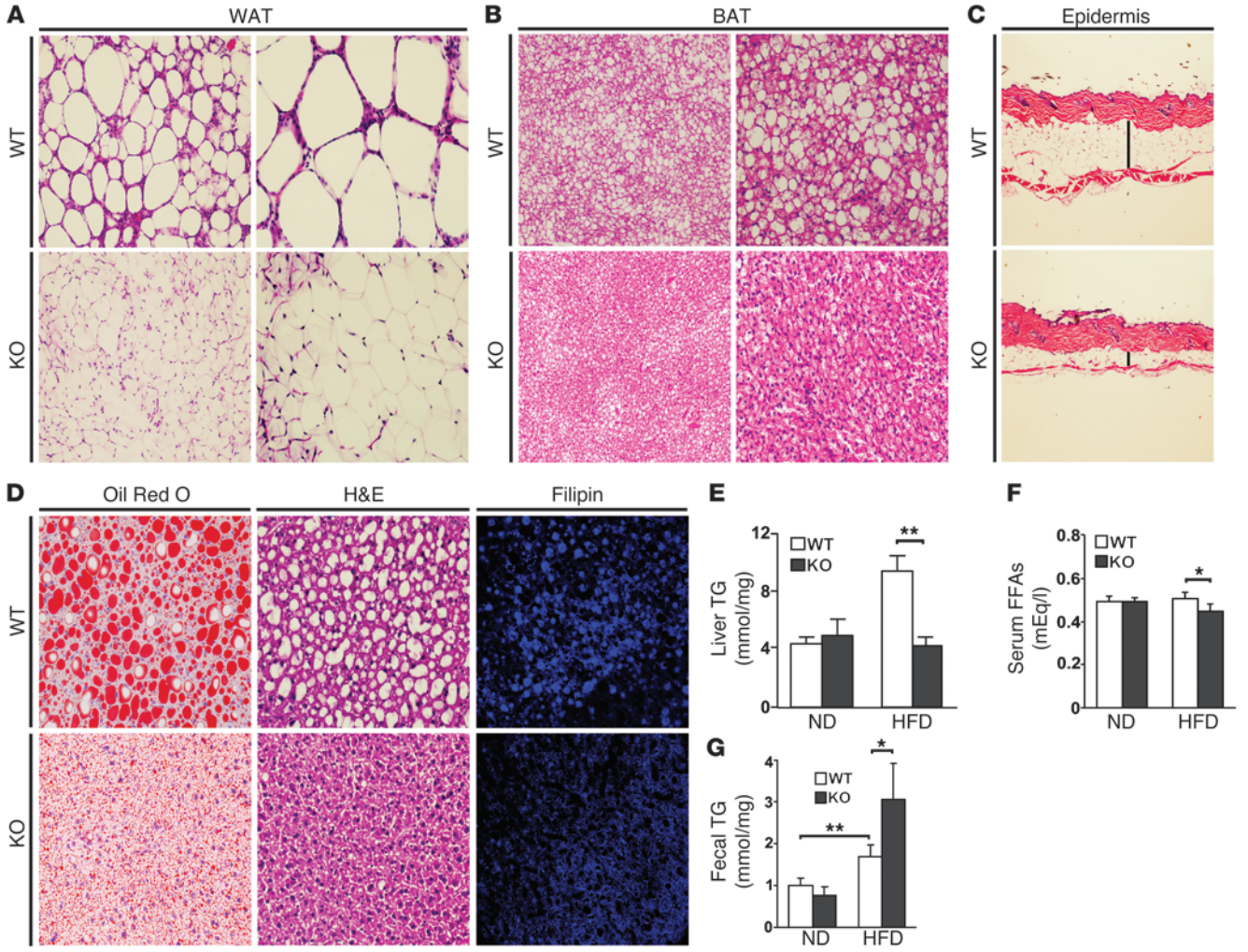

Figure 3

Parkin$^{-/-}$ mice are resistant to HFD-induced fat accumulation. Tissue sections were analyzed after 6.5 weeks of the HFD. WAT (**A**) and BAT (**B**) were processed using H&E staining. The upper panels show *Parkin*$^{+/+}$ (WT) mice and lower panels show *Parkin*$^{-/-}$ (KO) mice. Original magnification, ×10 (left panels); ×20 (right panels). (**C**) The skin epidermal thickness in transverse sections from *Parkin*$^{+/+}$ and *Parkin*$^{-/-}$ mice (H&E staining). Vertical line shows the subcutaneous fat. (**D**) TG accumulation in liver sections by Oil Red O and H&E staining, and cholesterol levels by Filipin staining in Parkin WT and *Parkin*$^{-/-}$ mice. Original magnification, ×20 (left panels); ×20 (middle panels); ×40 (right panels).(**E**) Hepatic TG levels, (**F**) serum-free fatty acid levels, and (**G**) TG levels in the feces on the ND and HFD comparing the WT and KO mice. The feces from the mice fed a ND (n = 4) or HFD (n = 7) for 5 weeks were collected daily over a 3-day period. Lipids were extracted from the feces and TG measured using a colorimetric assay. Data are expressed as mean ± SD. Representative histological images are shown; similar results were acquired from 3–4 independent mice. *P < 0.05; **P < 0.01 versus controls (n = 4–7 per group).

ning this, we measured the accumulation of long-chain fatty acids in response to Parkin manipulation and oleate administration. The cellular neutral lipid levels were markedly lower in *Parkin*$^{-/-}$ MEF cells compared with WT MEF cells in response to BSA-conjugated oleic acid (0.5 and 1 mM) over a 24-hour period (Figure 4A). Gain-of-function studies were performed in HepG2 cells after transfection with full-length WT Parkin and ubiquitin-like domain-deleted Parkin (ΔUbi-Parkin), respectively (Figure 4B). Overexpression of full-length Parkin increased oleic acid accumulation, and intriguingly, the capacity to increase oleic acid uptake was prevented by the absence of the ubiquitin-like domain of Parkin (Figure 4C). We then confirmed that the overexpression of full-length Parkin could increase fat uptake by performing a kinetic assay with fluorescent-labeled palmitate (Figure 4D and Supplemental Figure 3). To assess whether this Parkin regulatory program is operational in neurons, we investigated fat uptake in human neuroblastoma SH-SY5Y cells. Fat levels were again augmented following the overexpression of full-length Parkin, but the overexpression of ubiquitin-like domain-deleted Parkin prevented oleate accumulation (Figure 4E). To evaluate whether this phenotype is operational in the context of *PARK2* mutations that predispose to PD, we studied transformed B cell lines "banked" from patients with complex heterozygous or homozygous *PARK2* mutations that presented with premature onset Parkinsonism (21). In keeping with the reduced accumulation of oleic acid in the *Parkin*$^{-/-}$ MEF cells, all 3 Parkin mutant subject cell lines showed diminished accumulation of oleic acid compared with 4 control cell lines (Figure 4F).

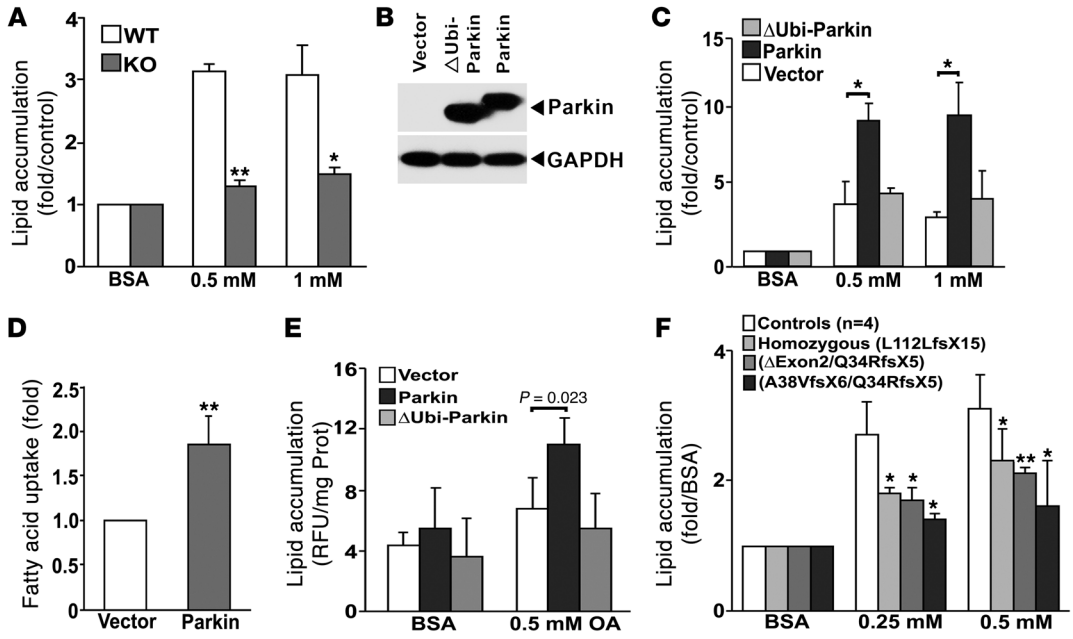

Figure 4

Parkin modulation of lipid uptake requires an intact ubiquitin-like domain. (**A**) Lipid accumulation assayed by Nile red staining in MEFs from *Parkin*$^{+/+}$ (WT) and *Parkin*$^{-/-}$ (KO) after BSA-conjugated oleate (0.5 and 1 mM) incubation. Values represent the fold relative to BSA incubation and normalized to cell number. The values represent the average of 5 independent experiments. (**B**) Parkin expression in HepG2 cells overexpressing vector, WT Parkin, and ΔUbi-Parkin constructs. (**C**) Lipid accumulation in HepG2 cells overexpressing vector, Parkin, and ΔUbi-Parkin after oleate incubation (0.5 and 1 mM). (**D**) Relative fluorescence of Bodipy-labeled dodecanoic acid at the end of 1,200-second incubation in HepG2 cells overexpressing Parkin compared with vector controls. Values represent the fold relative to vector-transfected HepG2 cells. (**E**) Lipid accumulation in SH-SY5Y neuroblastoma cells overexpressing vector, Parkin, and ΔUbi-Parkin after 0.5 mM oleate incubation. Values are normalized to protein concentration. (**F**) Lipid accumulation in response to 0.25 and 0.5 mM oleate in transformed B cells from 3 patients with *PARK2* mutations versus 4 WT control subjects. Values were normalized to cell number. Data are displayed relative to control cells exposed to BSA normalized to 1. Data are expressed as mean ± SD. **P* < 0.05; ***P* < 0.01 versus control or vector.

Parkin expression is nutrient responsive and regulates lipid transport protein levels. To further explore the mechanism underlying the regulatory role of Parkin on lipid uptake, we assessed hepatic Parkin levels in response to altered dietary composition. In *Parkin*$^{+/+}$ mice, steady-state Parkin was expressed at low levels but was robustly induced following HFD feeding (Figure 5A). Interestingly, the protein levels of the lipid uptake and transport proteins CD36, Sr-B1, and L-FABP were also increased in the liver of WT mice in response to the HFD. However, these lipid uptake and transport proteins were not induced by HFD in *Parkin*$^{-/-}$ mice (Figure 5A). Although these hepatic protein changes were not faithfully replicated at the transcript level (Supplemental Figure 4A), the induction of Parkin and CD36 protein levels in response to the HFD were evident in the brain of WT mice (Figure 5B). In contrast to the liver, the neuronal expression of Sr-B1 and B-FABP did not parallel the nutrient-dependent changes in Parkin expression (Figure 5B). As CD36 levels paralleled Parkin expression in multiple tissues, we evaluated whether Parkin modulates CD36 protein stability. The temporal CD36 steady-state protein levels were assessed following cycloheximide (CHX) administration with or without the overexpression of Parkin in HeLa cells engineered to constitutively express CD36 (22). Increased Parkin resulted in the maintenance of CD36 protein levels compared with the rate of degradation in control vector–transfected cells (Figure 5C). According to the prior studies showing that the administration of fatty acids diminished CD36 levels in cell culture studies (23), we explored whether Parkin modulates CD36 expression in the presence of oleic acid. We showed that oleic acid treatment reduced CD36 expression in control vector–transfected cells. However, the overexpression of Parkin in the presence of vehicle (BSA) modestly increased CD36 levels with relatively higher protein levels in the presence of oleic acid (Figure 5D). We then investigated whether Parkin functionally interacts with CD36. IP of Flag-tagged Parkin and subsequent immunoblot analysis for CD36 supported the physical interaction between Parkin and CD36 (Figure 5E). To evaluate whether Parkin directly ubiquitinates CD36, the concurrent overexpression of Parkin and HA-tagged ubiquitin constructs was performed and the antibody directed against ubiquitinated lysine residues and CD36 was used in IP assays. Reciprocal immunoblot analysis showed that Parkin increased ubiquitination of CD36 when Parkin and WT ubiquitin (Ubi-WT) were concurrently overexpressed (Figure 5, F and G). To begin to assess whether a higher molecular weight band resulted from the possible monoubiquitination of CD36, the input immunoblot was exposed for a longer duration. A higher molecular weight band was evident immediately above the expected size of CD36 when Parkin was coexpressed with ubiquitin (Supplemental Figure 4B). A possible consequence of Parkin-induced CD36 steady state levels could manifest with increased cell surface CD36 levels to facilitate increased fatty acid uptake. We measured endogenous CD36 membrane localization using flow cytometry with a

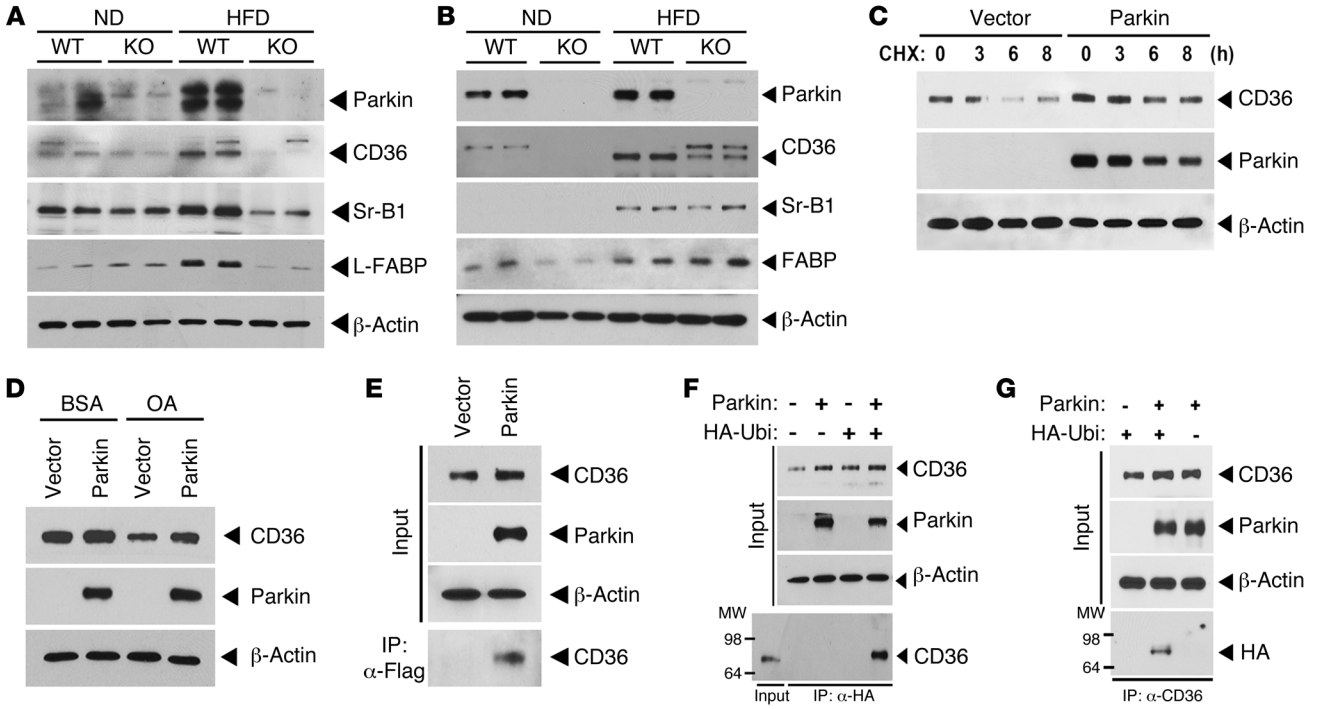

Figure 5

Parkin regulates posttranslational modification of CD36. (**A**) Expression levels of Parkin and lipid uptake (CD36 and Sr-B1) and transport (L-FABP) proteins in response to the ND and HFD in liver tissue by immunoblot analysis. (**B**) Protein expression of Parkin and lipid uptake and transport proteins in response to the ND and HFD in whole brain tissue by immunoblot analysis. (**C**) Degradation of CD36 protein following CHX administration in the presence or absence of Parkin overexpression in HeLa cells engineered to overexpress CD36. (**D**) CD36 protein expression in response to oleic acid administration following overexpression of Parkin or control vector. (**E**) Interaction between Parkin and CD36. CD36-overexpressing HeLa cells were transfected with p3×Flag vector or p3×Flag-Parkin, respectively. After 48 hours transfection, protein extracts were IP with anti-Flag M2 agarose (IP:α-Flag). (**F**) Ubiquitination of CD36 following IP of an HA antibody and immunoblot analysis for CD36. CD36-overexpressing HeLa cells were transfected with HA-Ubiquitin and/or Parkin. (**G**) Ubiquitination of CD36 following IP with a CD36 antibody and immunoblot analysis for HA following the transfection of HA-Ubiquitin and/or Parkin in the CD36-overexpressing HeLa cells. All studies were performed in duplicate, and at least 3 independent experiments were performed.

fluorescence antibody directed at cell membrane CD36 in HepG2 cells following transient overexpression of the empty vector versus the WT Parkin construct. Here, the overexpression of Parkin increased membrane localization of CD36 in excess of 3-fold (Supplemental Figure 4C). In parallel with the investigation of the functional consequences and interaction of Parkin with CD36, we investigated the interaction of Parkin with Sr-B1. We show that Parkin and Sr-B1 functionally interact as assessed by IP studies (Supplemental Figure 4D) and that Sr-B1 protein levels were maintained by Parkin overexpression (Supplemental Figure 4E). However, we were unable to demonstrate a direct role of Parkin in the ubiquitination of Sr-B1 (data not shown).

The reconstitution of CD36 and Parkin restores hepatic lipid uptake. To further explore this interaction between Parkin and CD36, we evaluated whether the augmentation of CD36 in *Parkin*$^{-/-}$ mouse liver could increase fat uptake and whether the reconstitution of Parkin in *Cd36*$^{-/-}$ primary hepatocytes could similarly modulate this biology. The levels of hepatic CD36 following viral infection with CD36 versus the GFP viral particles were robustly increased in both Parkin WT and *Parkin*$^{-/-}$ mice (Figure 6A). Following an overnight fast, the mice received an intravenous bolus of purified TG-rich VLDL particles. Livers were extracted approximately 2.5 hours later to assess hepatic fat accumulation. Hepatic lipid stores were significantly increased in Parkin WT and *Parkin*$^{-/-}$ mice following infection with CD36 compared with GFP control viral particles (Figure 6B and Supplemental Figure 5A). To evaluate whether the effect of Parkin was exclusively due to the stability of CD36, we cultured primary hepatocytes from *Cd36*$^{+/+}$ and *Cd36*$^{-/-}$ mice and infected them with adenoviral particles harboring GFP control or Parkin expression vectors (Figure 6C). At baseline, ^{14}C-labeled oleic acid was significantly higher in the *Cd36*$^{+/+}$ hepatocytes (Figure 6D). Although the amount of fat uptake in *Cd36*$^{-/-}$ hepatocytes were markedly lower than in *Cd36*$^{+/+}$ cells, Parkin overexpression significantly increased fat uptake in both primary hepatocyte genotypes (Figure 6D and Supplemental Figure 5B). We similarly evaluated whether Parkin reconstitution would rescue fat uptake in the *Parkin*$^{-/-}$ mice. Here, mice were infected with adenovirus particles harboring Parkin or a GFP control vector. In parallel with the primary hepatocyte and cell transfection studies, the reconstitution of Parkin increased neutral lipid levels in the *Parkin*$^{-/-}$ mouse livers as assessed following an intravenous infusion of TG-rich VLDL. Of note, the augmentation of Parkin in WT mice in these acute studies did not further increase neutral lipid accumulation (Figure 6E). Viral infection efficiency was shown by immunoblot analysis of Parkin and GFP (Supplemental Figure 5C). In order to evaluate whether the reconstitution of

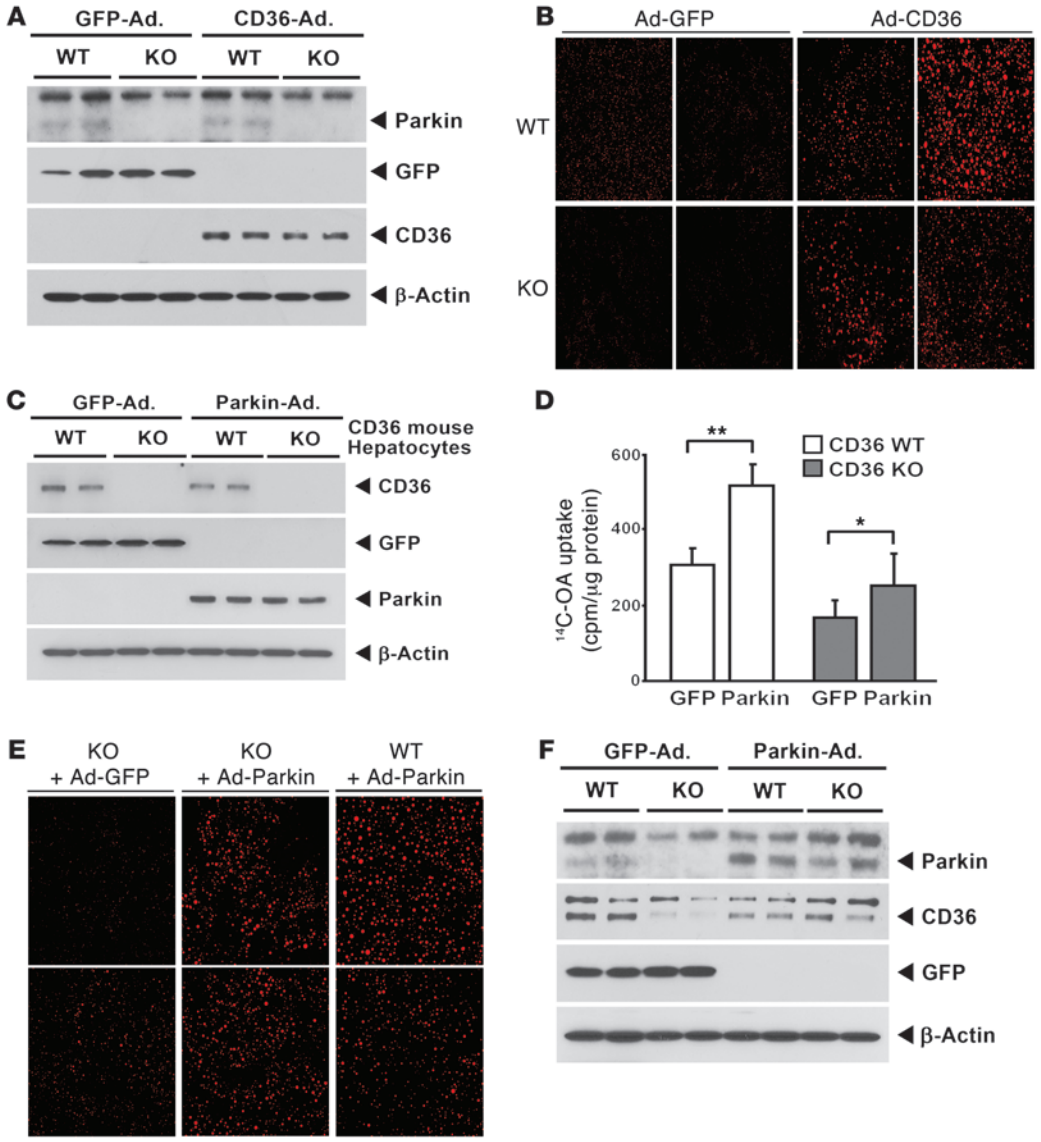

Figure 6

Fat uptake is enhanced following reconstitution of CD36 or Parkin. (**A**) Immunoblot analysis showing overexpression of CD36 versus GFP control adenovirus (Ad) in *Parkin*$^{+/+}$ and *Parkin*$^{-/-}$ mice liver. A short exposure of the CD36 immunoblot bands is shown to maintain the viral overexpression levels within the linear range. (**B**) Confocal microscopy of fixed liver tissue showing enhanced VLDL uptake following CD36 infection (red fluorescence). Representative fat levels are shown in 2 *Parkin*$^{+/+}$ and *Parkin*$^{-/-}$ mice following either GFP or CD36 adenoviral infection. Original magnification, ×40. (**C**) Immunoblot analysis showing GFP or Parkin expression in *Cd36*$^{+/+}$ and *Cd36*$^{-/-}$ primary hepatocytes following either GFP or Parkin adenoviral infection. (**D**) Radiolabeled oleate uptake in *Cd36*$^{+/+}$ and *Cd36*$^{-/-}$ primary hepatocytes. Data are expressed as mean ± SD. *$P < 0.05$; **$P < 0.01$ versus controls. (**E**) Confocal microscopy showing enhanced VLDL uptake following Parkin infection in mouse livers. Original magnification, ×40. (**F**) Immunoblot analysis showing induction of Parkin and CD36 in Parkin WT and *Parkin*$^{-/-}$ mice on the HFD following infection with Parkin or GFP adenoviral particles.

Parkin would increase hepatic CD36 levels, mice were fed the HFD for 6 days in conjunction with the viral infection studies. As shown in Figure 6F, the reconstitution of Parkin increased CD36 levels in the liver of *Parkin*$^{-/-}$ mice without a significant change in protein levels in the *Parkin*$^{+/+}$ mice.

The role of Parkin in fat accumulation is similarly evident during adipogenesis. The HFD studies show that Parkin deficiency diminished fat levels in multiple organs, and our genetic manipulation studies support the role of Parkin in fat uptake in MEFs, hepatocytes, and neuronal cells. To evaluate whether the lack of Parkin directly affects cellular processes dependent on fat uptake, we explored whether Parkin was required for fat accumulation during adipogenesis. To determine this, *Parkin*$^{+/+}$ and *Parkin*$^{-/-}$ MEFs and 3T3-L1 cells were employed in adipocyte differentiation studies. Interestingly, Parkin and CD36 protein levels were robustly upregulated during adipocyte differentiation in WT MEFs (Figure 7, A and B). After adipocyte differentiation of primary MEFs, the level of fat accumulation was significantly

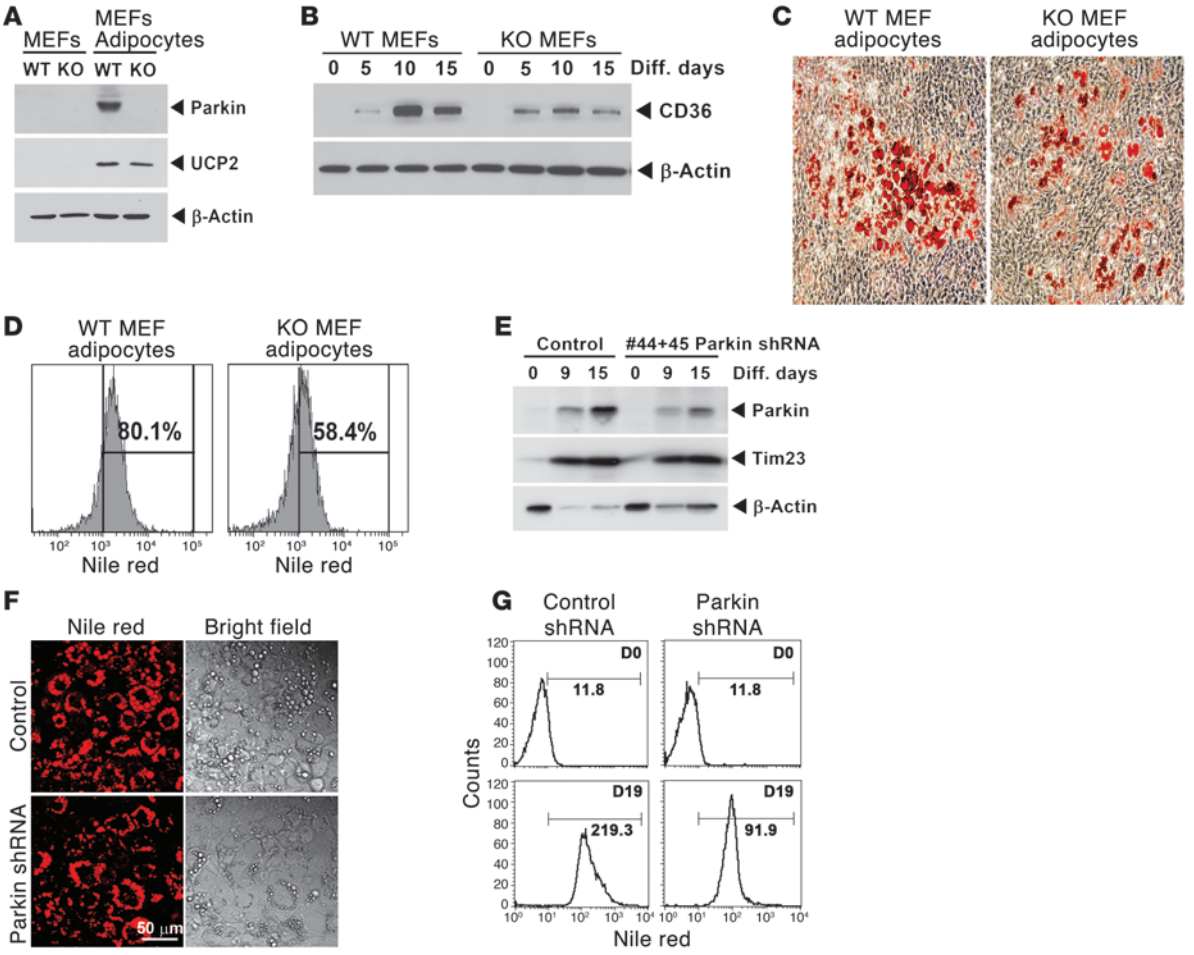

Figure 7

Parkin is regulated in parallel with fat accumulation in adipocytes and functions to facilitate fat uptake during adipogenesis. (**A**) Representative immunoblot showing increased Parkin expression in *Parkin*$^{+/+}$ MEF cells on day 21 adipocyte differentiation. The ubiquitously expressed mitochondrial uncoupling protein 2 (UCP2) is increased during adipogenesis in both *Parkin*$^{+/+}$ and *Parkin*$^{-/-}$ MEF cells. (**B**) Representative immunoblot showing the temporal induction of CD36 levels in *Parkin*$^{+/+}$ and *Parkin*$^{-/-}$ MEFs. β-actin levels reflect protein loading. (**C**) Light microscopy shows Oil Red O staining on day 21 adipocyte differentiation in MEFs with increased staining in Parkin WT MEFs. Original magnification, ×10. (**D**) Representative flow cytometric profile showing Nile red uptake in differentiated MEF cells to compare cellular fat accumulation. The percentages shown represent the increase in neutral lipid accumulation above predifferentiated MEF cell levels. (**E**) Immunoblot analysis of 3T3-L1 cell differentiation with higher Parkin levels in the scrambled shRNA-treated cells versus those transfected with 2 Parkin shRNAs. The inner mitochondrial membrane transport protein (Tim23) is increased during adipogenesis and shows similar expression in control and Parkin shRNA–treated cells. (**F**) Light microscopy to show fat accumulation in differentiated 3T3-L1 adipocytes by Nile red or by bright-field microscopy comparing control and Parkin shRNA–infected cells. Original magnification, ×20. (**G**) Flow cytometry showing significantly more neutral lipid accumulation in control versus Parkin shRNA–infected 3T3-L1 cell adipocyte differentiation on day 19 (D19) versus the cytometric profile prior to differentiation (D0). The numbers adjacent to the distribution curves represent the geometric mean of fluorescence intensity in the cell populations gated to measure Nile red accumulation. All experiments were repeated 3 or more times.

higher in the adipocytes of *Parkin*$^{+/+}$ MEFs compared with the KO MEFs as measured by Oil Red O (Figure 7C and Supplemental Figure 6A) and by Nile red staining (Figure 7D). This finding was replicated during 3T3-L1 cell differentiation into adipocytes, where Parkin levels increased with progressive adipocyte differentiation (Figure 7E), and the concurrent knockdown of Parkin prior to differentiation attenuated fat accumulation in 3T3-L1 adipocytes (Figure 7, F and G) In addition, the level of attenuated fat accumulation paralleled the level of Parkin knockdown (Supplemental Figure 6, B and C).

Discussion

As mutations in *PARK2* present with premature-onset PD, a large number of studies have investigated its function in neuronal biology. Although initial characterization of the *Parkin*$^{-/-}$ mouse demonstrated perturbations in synaptic excitability, the expected loss of substantia nigra neurons characteristic of PD was not evident in the analysis of these mice up to the age of 24 months (2). This observation spurred more expansive investigations into the functional role of Parkin and raised questions regarding an exclusive role in dopaminergic tissues.

A broader biological role for Parkin is similarly suggested, as the Parkin transcript is ubiquitously expressed and shows the highest levels in metabolically active tissues (24). The extraneuronal function of Parkin was unmasked when the Parkin ortholog was genetically disrupted in drosophila (25). These flies showed numerous systemic defects, with a diminished body mass and a profound disruption in flight muscle mitochondria. The role of Parkin in the control of mitochondrial homeostasis has expanded, as aging *Parkin*$^{-/-}$ mice also display diminished neuronal mitochondrial oxidative phosphorylation protein levels in parallel with increased oxidative stress and blunted mitochondrial respiration (20). Parkin also translocates to de-energized mitochondria to initiate mitophagy (8) and has been implicated in the control of mitochondrial dynamics (26). However, we did not observe significant changes in the liver mitochondrial proteome comparing Parkin WT and *Parkin*$^{-/-}$ mice at 3 months of age (data not shown). In light of these negative findings, we reasoned that the previously recognized lack of weight gain evident in the young *Parkin*$^{-/-}$ mice (20) was unlikely to be due to a primary mitochondrial defect. This was further supported in our study, as basal indirect calorimetry and the response to a hypothermic challenge were similar in comparing the Parkin WT and *Parkin*$^{-/-}$ mice.

E3-ligase–mediated ubiquitination of substrate proteins promotes polyubiquitination with subsequent proteosomal degradation and/or mono and multi-monoubiquitination to modify protein function and stability (27, 28). This role of monoubiquitination is illustrated where monoubiquitination of phosphoenolpyruvate carboxylase modifies enzymatic allosteric and kinetic properties (29). Interestingly, other E3 ubiquitin ligase enzymes have been identified in the modulation of lipid biology (30) and in altering resistance to HFD-induced weight gain and insulin resistance (31, 32). In those studies, E3 ubiquitin ligases promoted degradation of the LDL receptor and increased levels of metabolic enzymes and uncoupling proteins, respectively (30, 31). The substrates targeted by Parkin to date are limited (33–37), although degradation-independent ubiquitination has been identified with automultimonoubiquitination of Parkin itself and the multimonoubiquitination of Hsp70 (14, 33, 38). Our data add a new target to this growing list of substrates, showing that CD36 ubiquitination by Parkin leads to increased protein stability in cell culture studies, in WT mice in parallel with the upregulation of Parkin, and following the reconstitution of this E3 ligase in the *Parkin*$^{-/-}$ mice. The target residues and pattern of Parkin-mediated ubiquitination of CD36 and the direct functional consequences of this posttranslational modification are actively being explored in the laboratory.

CD36 has previously been shown to be ubiquitinated in CHO cells and in C2C12 myotubes by fatty acids, which results in diminution in protein stability (23). We show that CD36 protein levels are increased following a HFD in endogenous liver tissue in parallel with the upregulation of Parkin and in CD36-expressing HeLa cells following Parkin overexpression. Interestingly, in these HeLa cells, exposure to oleic acid alone also reduces CD36 levels, whereas the introduction of Parkin prevents this oleate-mediated reduction in CD36 levels. The role of Parkin in increasing CD36 stability was further supported by the increased steady-state levels following CHX administration. Together, these data support that the upregulation of Parkin in WT mice in response to HFD feeding and the introduction of Parkin in cell studies and in the *Parkin*$^{-/-}$ mouse modify the ubiquitination process to enhance the stability of this fatty acid transport protein. Although this study focused on CD36 as a target of Parkin regulation, the concomitant upregulation of Sr-B1 and FABP in the liver suggest that this lipid uptake regulatory program extends beyond the exclusive modulation of CD36. This is additionally supported by the capacity, albeit at a lower level, for Parkin to augment fat uptake in the *Cd36*$^{-/-}$ hepatocytes and in that the *Parkin*$^{-/-}$ mice do not faithfully phenocopy *Cd36*$^{-/-}$ mice (39).

In the same context, the blunted weight gain in *Parkin*$^{-/-}$ mice is probably due to systemic effects of Parkin and not restricted to a single organ. This is supported by reduced fat uptake in *Parkin*$^{-/-}$ MEFs, during MEF and 3T3-L1 cell differentiation into adipocytes, and in Parkin mutant patient transformed B cells. The systemic effect of Parkin is further supported in that lipid levels are disproportionately higher in the feces of *Parkin*$^{-/-}$ mice on the HFD than in the WT controls. These systemic and possibly neuronal effects of Parkin on lipid uptake warrant further exploration and may be important in the pathophysiology of premature PD.

The 3 PD patient cell lines interrogated in this study possess frameshift mutations or deletion of exons 2 or 3 of *PARK2* (21). These mutations either disrupt the N-terminal ubiquitin-like (Ubl) domain or the immediate flanking linker region. The Ubl domain is the same region that is deleted in the ubiquitin-like domain mutant construct we employed (40), showing the requirement of this domain in enhancing fat uptake. The Ubl domain has previously been shown to function as a SH3 domain–binding partner (36, 40), and the loss or dysfunction of this domain may be important to orchestrating the regulatory control of lipid uptake by Parkin. Interestingly, although mutations in Parkin are distributed across the whole protein, they predominate in the Ubl and RING domains (41). Whether mutations in the RING domain affect lipid metabolism and which domain interacts with CD36 have not been explored to date. Additionally, although mutations in Parkin are strongly associated with the development of premature PD (1, 41), the links between Parkin and either lipid disorders or metabolic syndromes are more tenuous. It is interesting to note, however, that the risk of developing diabetic nephropathy is associated with polymorphisms in *PARK2* (42). Also, an association between fat metabolism and a binding partner of Parkin, i.e., Pink1, has similarly been found (43), and whether this reflects a broader role of Parkin and its interacting partners in lipid metabolism is an emerging concept for future studies.

Finally, although the number of substrates of Parkin-mediated ubiquitination is increasing (33–36), the mechanisms underpinning Parkin function remain enigmatic. This study introduces a novel function of Parkin in the regulation of lipid biology that needs to be reconciled with the evidence supporting a role of Parkin in the control of mitochondrial homeostasis (8, 20, 26, 44). As the ratio and content of glycerol- and phospholipids in the mitochondria membrane are tightly controlled to maintain normal function, it would be of interest to evaluate whether the absence of, or mutations in *PARK2* evoke phenotypic features associated with the disruption of mitochondrial integrity due to perturbations in fat uptake.

In conclusion, this study demonstrates that Parkin modulates systemic lipid metabolism, in part, through the ubiquitination of CD36 resulting in increased protein stabilization and translocation to the plasma membrane with a concomitant increase in fat uptake. The role of Parkin in lipid biology is further supported by its regulation during adipogenesis and its requirement for fat lipid droplet accumulation in adipocytes. Although the predom-

inant focus of this study targeted the function of Parkin in the liver, serologic, adipose, neuronal, and fecal assays suggest a more widespread role of Parkin in modulating lipid metabolism. This biology requires additional characterization and may be useful in identifying additional substrates of Parkin. Finally, this study supports the direct investigation into whether perturbed lipid metabolism contributes to the pathophysiology of PD in patients with Parkin mutations.

Methods

Mice and diets. *Parkin*$^{-/-}$ mice (129/Sv×C57BL/6 background) were obtained from the Jackson Laboratory and bred using heterozygous pairing. At 12 weeks of age, the male mice were changed to either a ND or a HFD (Research Diets). The ND contained 20%, 70%, and 10% kcal as protein, carbohydrate, and fat and the HFD contained 20%, 20%, and 60% kcal as protein, carbohydrate, and fat, respectively. Cholesterol content of ND and HFD was 18 mg/kg food and 300.8 mg/kg food, respectively. *Cd36*$^{-/-}$ and control mice were maintained on the C57BL/6 Taconic background.

Cell culture studies. The Tet-on/off plasmid containing human CD36 and Sr-B1 was transfected into HeLa cells (human cervical adenocarcinoma). CD36- and Sr-B1–overexpressed stable HeLa cells were selected by Geneticin (Gibco; Invitrogen) treatment. HepG2 (human hepatoma cells), SH-SY5Y (human neuroblastoma cells), and 3T3-L1 (mouse fibroblasts) cells were obtained from ATCC. The transformed B cells from the PD patients (21) were purchased from Coriell Institute. *Parkin*$^{+/+}$ and *Parkin*$^{-/-}$ MEFs were generated from day 13.5 embryos after removing the head and internal organs. Adipogenesis studies were performed in early passage primary MEFs and 3T3L1 cells by exposing them to an induction medium (DMEM containing 10% FBS supplemented with 0.5 mM 3-isobutyl-1-methylxanthine, 1 μM dexamethasone, 10 μg/ml [MEFs] or 1 μg/ml [3T30L1 cells] insulin, and 0.5 μM rosiglitazone) for 48 hours (MEFs) or 72 hours (3T3-L1 cells). The medium was then replaced with DMEM containing 10% FBS, 5 μg/ml (MEFs), or 1 μg/ml (3T3-L1 cells) insulin, and 0.5 μM rosiglitazone (no rosiglitazone in 3T3-L1 cell differentiation medium) and changed on alternate days. The cells exhibited a fully differentiated phenotype with extensive accumulation of multiple fat droplets at 2–3 weeks after adipocyte induction. To study Parkin knockdown in 3T3-L1, cells were transducted with lentivirus carrying mouse Parkin shRNA (SHCLNV-NM_016694; Sigma-Aldrich). Cells were selected with medium containing 1 μg/ml puromycin for 7 days and cultured in medium without puromycin for 3 days before differentiation. Primary hepatocytes were isolated from *Cd36*$^{-/-}$ and *Cd36*$^{+/+}$ mice, as previously described (45). Briefly, livers were perfused with Leffert's buffer (10 mM HEPES, 3 mM KCl, 130 mM NaCl, 1 mM NaH_2PO_4, 10 mM D-glucose, pH 7.4) with 0.5 mM EGTA at 5 ml/min for 8 minutes, followed by continuous perfusion with digestion medium (90 units/ml collagenase I in Leffert's buffer with 0.0279% $CaCl_2$). The perfused livers were dissociated in ice-cold wash buffer (Leffert's buffer with 0.0279% $CaCl_2$) with forceps, and hepatocytes were plated on type I collagen–coated plates with culture medium (RPMI with 10% FBS, 100 nM dexamethasone and 1× ITS [Sigma-Aldrich]).

Plasmids and transfection. pcDNA plasmids encoding WT Parkin and ΔUbi-Parkin were obtained as gifts from Olga Corti (Pitié-Salpêtrière Hospital, Paris, France). The WT Parkin coding region was subcloned into p3xFlag vectors. The pRK5-HA-ubiquitin plasmid was purchased from Addgene. Transfections were performed with either Fugene HD (Roche) or Amaxa nucleofector (Lonza) according to the manufacturer's instructions.

Adenovirus preparation and injection. Full-length Parkin and CD36 cDNA constructs were subcloned into adenoviral vectors harboring the CMV promoter. The adenoviral vectors were transfected into 293 cells to generate recombinant adenovirus expressing Parkin (Ad-Parkin) and CD36 (Ad-CD36). The mice were infected by intravenous injection with 3×10^7 pfu virus/g BW. Four days after infection, mice were fasted for 20 hours; then human VLDL was administered (1 mg/mouse with Ad-CD36 and 1.5 mg/mouse with Ad-Parkin). Livers were extracted approximately 2.5 hours later to assess fat uptake. Adenovirus-expressing GFP (Ad-GFP, Vector Biolabs) was used as a control.

In vivo metabolic phenotype analysis. Mice were fed with a ND or a HFD for 5–6 weeks prior to the metabolic experiments. Mice were individually housed in the metabolic cage (Hatteras Instruments) and acclimatized for 2 days before data collection. Food and feces were weighed daily for 3 consecutive days. Fat mass was analyzed by nuclear magnetic resonance technology (NMR; Bruker). Oxygen consumption was measured by indirect calorimetry (Oxymax Columbus Instruments). Here, mice had ad libitum access to food and water and were singly housed 2 days prior to the experiment in air-proof plastic metabolic cages, connected to O_2 and CO_2 sensors. The Oxymax system allowed 4 individually housed animals to be monitored simultaneously. Energy expenditure and respiratory exchange ratio were measured for 24 hours at 10-minute intervals. Physical activity was measured using DSI (Data Sciences International) intraperitoneal embedded transmitters (TA10TA-F20). Activity data were collected over 3 days in the presence of food and water and performed in 4–7 mice per group. Body temperature response to hypothermia was measured by handheld transponders (BioMedic Data Systems) held next to BMDS chips that had previously been inserted into the mouse peritoneal cavity. Body temperature was measured every hour (0–5 hours) while mice were temporarily maintained in a 4°C ambient environment.

Analyses of tissue sections. After feeding for 6.5 weeks, mice were fasted for 18 hours and euthanized for isolating tissues. Liver tissues were frozen, sectioned in 5 μm, and stained with Oil Red O and H&E. Brown adipose tissue (BAT), white adipose tissue (WAT), and epidermis tissue were fixed in 10% neutral buffered formalin, processed into paraffin blocks, sectioned at 7 μm, and stained with H&E. Stained sections were examined by light microscopy (Olympus IX71). Liver cholesterol was assayed by staining with filipin (Sigma-Aldrich), a fluorescent polyene antibiotic, which binds specifically to the 3b-hydroxyl group of steroids. After viral infection, liver sections were labeled with neutral lipid Bodipy (Molecular Probes), GFP antibody (Invitrogen), and DAPI (Invitrogen). The sections were viewed by Leica SP1 or Zeiss LSM510 confocal microscopes.

Lipid extraction and measurement. Liver and feces (30–50 mg) were homogenized with chloroform/methanol (2:1) in a 20:1 v/w ratio using a TissueLyser (QIAGEN). After dispersion, the whole mixture was incubated overnight at 4°C with gentle shaking. Then, 0.2 volume of 0.9% NaCl was added and centrifuged at 500 *g* for 20 minutes (46). After extracting the organic phase, samples were evaporated under nitrogen until dry and reconstituted in PBS containing 1% Triton X-100 for TG measurement. For determining the cholesterol content, the dried samples were suspended in a solution of 28.75 mM PIPES, 57.51 mM $MgCl_2$, and 0.57 mg/ml BSA with 0.5% SDS and sonicated for 30 seconds (45). Concentration of TG and cholesterol from liver and feces was determined by colorimetric assay kits, respectively (BioVision).

GTT, ITT, and PTT. The mice were fed ND or HFD for 5 weeks. Mice were subjected to 16-hour fast for GTT and PTT and 6-hour fast for ITT, after which glucose (1.5 mg/g BW), insulin (0.75 mU/g BW), or pyruvate (2 mg/g BW), was administered by intraperitoneal injection. Blood glucose levels were measured at 0, 15, 30, 60, 90, and 120 minutes after injection by glucometer (Home Diagnostics). For measuring in vivo insulin signaling, the mice were fasted for 16 hours. Human recombinant insulin (20 units/kg) was administrated by intraperitoneal injection and the liver was isolated 15 minutes later for protein extraction and immunoblot analysis.

Blood biochemical assays. Blood was collected after 18 hours of fasting. Blood lipids and aminotransferase levels were measured by the Department of Laboratory Medicine at the NIH Clinical Center. Serum insulin and free fatty acids was determined by Ultra-Sensitive Mouse Insulin ELISA (Crystal Chem) and nonesterified fatty acids (Wako Diagnostics) kits.

Immunoblot analysis and IP. Total proteins from cells and tissues were extracted using RIPA buffer (50 mM Tris-HCl, pH 8.0, 0.5% deoxycholic acid, 1% NP-40, 0.1% sodium dodecyl sulfate, and 0.5 M NaCl) supplemented with protease inhibitor cocktails and phosphatase inhibitors (Sigma-Aldrich). The lysates were separated by 4%–20% or 10% Tris-glycine gel (Invitrogen) and transferred to nitrocellulose membranes. Antibodies were purchased from Cell Signaling (Parkin, ubiquitin, and phosphotyrosine), Sigma-Aldrich (Flag and β-actin), BD (Tim23), Biomol International (ubiquitin), Abcam (CD36, L-FABP, and B-FABP), R&D (CD36), Novus Biologicals (Sr-B1), Roche (HA), Chemicon (UCP-2), Millipore (IRβ), and Santa Cruz Biotechnology Inc. (HA, GAPDH and GFP). For IP, cells and liver tissues were extracted using the lysis buffer (50 mM Tris-HCl, pH 7.4, 1% Triton X-100, 0.5% NP-40, and 0.5 M NaCl) containing protease inhibitor cocktails and phosphatase inhibitors. Protein extract was incubated with antibodies against ubiquitin, CD36, HA, IRβ or anti-Flag M2 agarose (Sigma-Aldrich) overnight at 4°C. For antibody conjugates, protein G agarose (Sigma-Aldrich) was added and incubated for 4 hours. The agarose beads were washed with RIPA buffer and boiled in sample loading buffer. The supernatant was used for immunoblot analysis.

Protein stability assay. CD36- and Sr-B1–overexpressing HeLa cells were transfected with vector and WT Parkin plasmid, respectively. After 48 hours transfection, the cells were treated with 5 μg/ml CHX (Sigma-Aldrich) for the indicated times and proteins were extracted. Protein degradation was determined by immunoblot analysis.

Lipid droplet staining. Cells were incubated with oleic acid (Sigma-Aldrich) conjugated with 1% BSA overnight and stained with 10 μg/ml Nile red (Sigma-Aldrich) for 10 minutes in PBS. After washing with PBS, cells were read at 485 nm excitation/535 nm emission by a Tecan microplate reader. Values were normalized to cell number or protein concentration. The mean value was determined from 4 independent experiments, and the measurement was performed in quadruplicate for each experiment. After adipocyte differentiation, cells were fixed in 10% formalin for 10 minutes and stained with a filtered 0.2% Oil Red O solution for 15 minutes. Excess stain was removed by washing with water and visualized by light microscopy. The cells were then incubated for 10 minutes with isopropyl alcohol, which dissolved stained lipid droplets. The absorbance of the dye was measured at 495 nm. Values were normalized to protein concentration.

Flow cytometry. The cells were incubated with FITC-conjugated CD36 antibody (CB38 clone; BD Biosciences) and Nile red (10 μg/ml), respectively. A mouse IgM conjugated with FITC was used as an isotype control of CD36 antibody. The cells were analyzed using the FACSCanto (BD).

Fatty acid uptake assay. HepG2 cells were plated at 5×10^4 per well in 96-well plates. Cells were incubated in serum-free HBSS medium overnight prior to assay. QBT fatty acid uptake assay kit (Molecular Devices) employs a bodipy–dodecanoic acid fluorescent fatty acid analog. Plate was read at 485 nm excitation/535 nm emission with bottom-read mode by Tecan microplate reader. Kinetic assays were measured every 20 seconds for 1,200 seconds. Primary hepatocytes were plated on type I collagen–coated 6-well plates and infected with Ad-Parkin and Ad-GFP, respectively. On the next day, the cells were incubated with serum-free HBSS for 2 hours and 0.3% BSA conjugated with 50 μM ^{14}C-Oleic acid (American Radiolabeled Chemicals) and 100 μM oleic acid was added. After 30 minutes incubation, cells were lysed with 0.1% Triton X-100 and measured by β-scintillation counter. Values were normalized to protein concentration.

VLDL isolation. VLDL (d<1.019) fraction was isolated from fresh human plasma by density gradient ultracentrifugation as previously described (47). It was dialyzed against 150 mM NaCl and 0.01% EDTA. The concentration was determined by the Bradford method.

Quantitative real-time PCR. Total RNA was isolated from liver using RNeasy Mini Kit (QIAGEN). Reverse transcription of total RNA was performed using SuperScript III first-strand synthesis system (Invitrogen) according to the manufacturer's protocol. Quantitative real-time PCR was performed using SYBR Green PCR Master Mix (Applied Biosystems) and run on Opticon2 DNA engine (Bio-Rad). All reactions were normalized using an 18S endogenous control. Primers were purchased from predesigned primers of QuantiTect primer assays (QIAGEN).

Statistics. Data are expressed as mean ± SD for the indicated number of observations. Statistical significance between groups was determined using 2-tailed Student's *t* test when analyzing the dietary groups or within a single genotype. Multiple comparison analysis was performed using ANOVA. $P < 0.05$ was considered statistically significant.

Study approval. All mouse experiments were performed in accordance with a protocol approved by the NHLBI Division of Intramural Research Animal Care and Use Committee.

Acknowledgments

We thank Paul Hwang, Mark Knepper, Joe Chou, and Jay Chung, all of the NHLBI, for the generous use of their metabolic analysis equipment. We acknowledge the technical assistance of Jie Liu, Ilsa Rovira, and Liu Cao (NHLBI). We also thank Sonja Scholz (NIA) for helpful discussions about the human B cell lines; Bob Shamburek (NHLBI) and Oksana Gavrilova (NIDDK) for helpful suggestions regarding lipid biology; and Toren Finkel for helpful discussion about the manuscript. Finally, we thank Olga Corti from Pitié-Salpêtrière Hospital (France) for the pcDNA-Parkin/ΔUbi constructs. This research was funded by the Division of Intramural Research program of the NHLBI. S. Rusk and R. Huang were supported by the Howard Hughes Medical Institute/NIH research Fellowship and the NIH/Pfizer Clinical Research Training Program, respectively.

Received for publication August 12, 2010, and accepted in revised form July 20, 2011.

Address correspondence to: Michael N. Sack, Center for Molecular Medicine, NHLBI, Building 10-CRC, Room 5-3150, 10 Center Drive, Bethesda, Maryland, 20892-1454, USA. Phone: 301.402.9259; Fax: 301.480.4599; E-mail: sackm@nhlbi.nih.gov.

1. Kitada T, et al. Mutations in the parkin gene cause autosomal recessive juvenile parkinsonism. *Nature*. 1998;392(6676):605–608.
2. Goldberg MS, et al. Parkin-deficient mice exhibit nigrostriatal deficits but not loss of dopaminergic neurons. *J Biol Chem*. 2003;278(44):43628–43635.
3. Perez FA, Palmiter RD. Parkin-deficient mice are not a robust model of parkinsonism. *Proc Natl Acad Sci U S A*. 2005;102(6):2174–2179.
4. Kitada T, Tong Y, Gautier CA, Shen J. Absence of nigral degeneration in aged parkin/DJ-1/PINK1 triple knockout mice. *J Neurochem*. 2009;111(3):696–702.
5. Beasley SA, Hristova VA, Shaw GS. Structure of the Parkin in-between-ring domain provides insights for E3-ligase dysfunction in autosomal recessive Parkinson's disease. *Proc Natl Acad Sci U S A*. 2007;104(9):3095–3100.
6. Suzuki H. Protein-protein interactions in the mammalian brain. *J Physiol*. 2006;575(pt 2):373–377.
7. da Costa CA, et al. Transcriptional repression of p53 by parkin and impairment by mutations associated with autosomal recessive juvenile Parkinson's disease. *Nat Cell Biol*. 2009;11(11):1370–1375.
8. Narendra D, Tanaka A, Suen DF, Youle RJ. Parkin is recruited selectively to impaired mitochondria and promotes their autophagy. *J Cell Biol*. 2008;183(5):795–803.
9. Geisler S, et al. PINK1/Parkin-mediated mitophagy is dependent on VDAC1 and p62/SQSTM1. *Nat Cell Biol*. 2010;12(2):119–131.
10. Shimura H, et al. Familial Parkinson disease gene product, parkin, is a ubiquitin-protein ligase. *Nat*

Genet. 2000;25(3):302–305.
11. Lim KL, et al. Parkin mediates nonclassical, proteasomal-independent ubiquitination of synphilin-1: implications for Lewy body formation. *J Neurosci.* 2005;25(8):2002–2009.
12. Fallon L, et al. A regulated interaction with the UIM protein Eps15 implicates parkin in EGF receptor trafficking and PI(3)K-Akt signalling. *Nat Cell Biol.* 2006;8(8):834–842.
13. Xiong H, et al. Parkin, PINK1, and DJ-1 form a ubiquitin E3 ligase complex promoting unfolded protein degradation. *J Clin Invest.* 2009;119(3):650–660.
14. Moore DJ, West AB, Dikeman DA, Dawson VL, Dawson TM. Parkin mediates the degradation-independent ubiquitination of Hsp70. *J Neurochem.* 2008;105(5):1806–1819.
15. Huang X, Abbott RD, Petrovitch H, Mailman RB, Ross GW. Low LDL cholesterol and increased risk of Parkinson's disease: prospective results from Honolulu-Asia aging study. *Mov Disord.* 2008;23(7):1013–1018.
16. de Lau LM, Bornebroek M, Witteman JC, Hofman A, Koudstaal PJ, Breteler MM. Dietary fatty acids and the risk of Parkinson disease: the Rotterdam study. *Neurology.* 2005;64(12):2040–2045.
17. de Lau LM, Koudstaal PJ, Hofman A, Breteler MM. Serum cholesterol levels and the risk of Parkinson's disease. *Am J Epidemiol.* 2006;164(10):998–1002.
18. Ross BM, Moszczynska A, Erlich J, Kish SJ. Low activity of key phospholipid catabolic and anabolic enzymes in human substantia nigra: possible implications for Parkinson's disease. *NeuroScience.* 1998;83(3):791–798.
19. Willingham S, Outeiro TF, DeVit MJ, Lindquist SL, Muchowski PJ. Yeast genes that enhance the toxicity of a mutant huntingtin fragment or alpha-synuclein. *Science.* 2003;302(5651):1769–1772.
20. Palacino JJ, et al. Mitochondrial dysfunction and oxidative damage in parkin-deficient mice. *J Biol Chem.* 2004;279(18):18614–18622.
21. Brooks J, Ding J, Simon-Sanchez J, Paisan-Ruiz C, Singleton AB, Scholz SW. Parkin and PINK1 mutations in early-onset Parkinson's disease: comprehensive screening in publicly available cases and control. *J Med Genet.* 2009;46(6):375–381.
22. Baranova IN, et al. Role of human CD36 in bacterial recognition, phagocytosis, and pathogen-induced JNK-mediated signaling. *J Immunol.* 2008;181(10):7147–7156.
23. Smith J, Su X, El-Maghrabi R, Stahl PD, Abumrad NA. Opposite regulation of CD36 ubiquitination by fatty acids and insulin: effects on fatty acid uptake. *J Biol Chem.* 2008;283(20):13578–13585.
24. Cesari R, et al. Parkin, a gene implicated in autosomal recessive juvenile parkinsonism, is a candidate tumor suppressor gene on chromosome 6q25-q27. *Proc Natl Acad Sci U S A.* 2003;100(10):5956–5961.
25. Pesah Y, et al. Drosophila parkin mutants have decreased mass and cell size and increased sensitivity to oxygen radical stress. *Development.* 2004;131(9):2183–2194.
26. Lutz AK, et al. Loss of parkin or PINK1 function increases Drp1-dependent mitochondrial fragmentation. *J Biol Chem.* 2009;284(34):22938–22951.
27. O'Neill LA. Regulation of signaling by non-degradative ubiquitination. *J Biol Chem.* 2009;284(13):8209.
28. Yin H, Gui Y, Du G, Frohman MA, Zheng XL. Dependence of phospholipase D1 multi-monoubiquitination on its enzymatic activity and palmitoylation. *J Biol Chem.* 2010;285(18):13580–13588.
29. Uhrig RG, She YM, Leach CA, Plaxton WC. Regulatory monoubiquitination of phosphoenolpyruvate carboxylase in germinating castor oil seeds. *J Biol Chem.* 2008;283(44):29650–29657.
30. Zelcer N, Hong C, Boyadjian R, Tontonoz P. LXR regulates cholesterol uptake through Idol-dependent ubiquitination of the LDL receptor. *Science.* 2009;325(5936):100–104.
31. Molero JC, et al. c-Cbl-deficient mice have reduced adiposity, higher energy expenditure, and improved peripheral insulin action. *J Clin Invest.* 2004;114(9):1326–1333.
32. Molero JC, Turner N, Thien CB, Langdon WY, James DE, Cooney GJ. Genetic ablation of the c-Cbl ubiquitin ligase domain results in increased energy expenditure and improved insulin action. *Diabetes.* 2006;55(12):3411–3417.
33. Hampe C, Ardila-Osorio H, Fournier M, Brice A, Corti O. Biochemical analysis of Parkinson's disease-causing variants of Parkin, an E3 ubiquitin-protein ligase with monoubiquitylation capacity. *Hum Mol Genet.* 2006;15(13):2059–2075.
34. Huynh DP, Scoles DR, Nguyen D, Pulst SM. The autosomal recessive juvenile Parkinson disease gene product, parkin, interacts with and ubiquitinates synaptotagmin XI. *Hum Mol Genet.* 2003;12(20):2587–2597.
35. Ko HS, et al. Accumulation of the authentic parkin substrate aminoacyl-tRNA synthetase cofactor, p38/JTV-1, leads to catecholaminergic cell death. *J Neurosci.* 2005;25(35):7968–7978.
36. Trempe JF, et al. SH3 domains from a subset of BAR proteins define a Ubl-binding domain and implicate parkin in synaptic ubiquitination. *Mol Cell.* 2009;36(6):1034–1047.
37. Tanaka A, et al. Proteasome and p97 mediate mitophagy and degradation of mitofusins induced by Parkin. *J Cell Biol.* 2010;191(7):1367–1380.
38. Matsuda N, Kitami T, Suzuki T, Mizuno Y, Hattori N, Tanaka K. Diverse effects of pathogenic mutations of Parkin that catalyze multiple monoubiquitylation in vitro. *J Biol Chem.* 2006;281(6):3204–3209.
39. Hajri T, Han XX, Bonen A, Abumrad NA. Defective fatty acid uptake modulates insulin responsiveness and metabolic responses to diet in CD36-null mice. *J Clin Invest.* 2002;109(10):1381–1389.
40. Corti O, et al. The p38 subunit of the aminoacyl-tRNA synthetase complex is a Parkin substrate: linking protein biosynthesis and neurodegeneration. *Hum Mol Genet.* 2003;12(12):1427–1437.
41. Hedrich K, et al. Distribution, type, and origin of Parkin mutations: review and case studies. *Mov Disord.* 2004;19(10):1146–1157.
42. Leak TS, et al. Evaluation of a SNP map of 6q24-27 confirms diabetic nephropathy loci and identifies novel associations in type 2 diabetes patients with nephropathy from an African-American population. *Hum Genet.* 2008;124(1):63–71.
43. Franks PW, et al. Genomic variants at the PINK1 locus are associated with transcript abundance and plasma nonesterified fatty acid concentrations in European whites. *FASEB J.* 2008;22(9):3135–3145.
44. Narendra D, Tanaka A, Suen DF, Youle RJ. Parkin-induced mitophagy in the pathogenesis of Parkinson disease. *Autophagy.* 2009;5(5):706–708.
45. Jiang G, et al. Prevention of obesity in mice by antisense oligonucleotide inhibitors of stearoyl-CoA desaturase-1. *J Clin Invest.* 2005;115(4):1030–1038.
46. Rodriguez-Sureda V, Peinado-Onsurbe J. A procedure for measuring triacylglyceride and cholesterol content using a small amount of tissue. *Anal Biochem.* 2005;343(2):277–282.
47. Strachan AF, de Beer FC, van der Westhuyzen DR, Coetzee GA. Identification of three isoform patterns of human serum amyloid A protein. *Biochem J.* 1988;250(1):203–207.